第 29 卷第 1 期
2013 年 1 月

无 机 化 学 学 报
CHINESE JOURNAL OF INORGANIC CHEMISTRY

Vol.29 No.1
190-198

微波诱导燃烧法合成类花状 ZnO 纳米材料及其晶体结构、荧光性质研究

曹 渊* 文 毅 刘柏林 徐彦芹 王亚涛
(重庆大学化学化工学院,重庆 400030)

摘要: 以硝酸锌[$Zn(NO_3)_2\cdot 6H_2O$]和尿素[$CO(NH_2)_2$]作前驱体,通过微波诱导燃烧技术可控合成具有不同形貌的 ZnO 纳米晶体,并用热重分析和差热分析进行了研究。对各种生长条件:微波功率,辐射时间和尿素/Zn^{2+}物质的量的比对 ZnO 纳米晶体形貌的影响作了分析。结果表明:尿素/Zn^{2+}物质的量的比对 ZnO 纳米材料的形貌具有显著影响。X 衍射图表明合成的 ZnO 纳米结构呈六角形。傅里叶变换红外光谱图中 400~500 cm^{-1} 处明显的峰为 Zn-O 的振动峰。ZnO 纳米结构的发光光谱在 366 nm 的带边发射,因缺陷又由许多可见光发射峰组成。用扫描电子显微镜、透射电子显微镜、选区电子衍射研究了花状 ZnO 纳米结构的增长机理。本方法仅需几分钟就获得的了 ZnO 纳米结构。

关键词: ZnO; 微波燃烧; 纳米结构; 荧光
中图分类号: O611.4 **文献标识码**: A **文章编号**: 1001-4861(2013)01-0190-09
DOI:10.3969/j.issn.1001-4861.2013.00.023

Microstructures and Photoluminescence Property of Flower-Like ZnO Nanopowders Synthesized by Microwave-Induced Combustion Technique

CAO Yuan* WEN Yi LIU Bo-Lin XU Yan-Qin WANG Ya-Tao
(*College of Chemistry and Chemical Engineering, Chongqing University, Chongqing* 400030, *China*)

Abstract: ZnO crystals with different morphologies were controllably synthesized by the microwave-induced combustion technique. A solution of zinc nitrate [$Zn(NO_3)_2\cdot 6H_2O$] and urea [$CO(NH_2)_2$] was used as the precursor. The precursor of ZnO nanocrystal powders was studied by TG-DTA analysis. The effect of growth conditions, such as microwave power, radiation time, and urea/Zn^{2+} molar ratio, on the morphology of the ZnO nanocrystals was investigated. The results show that the molar ratio of urea/Zn^{2+} is the key factor affecting the morphology of the ZnO nanostructures. X-ray diffraction study indicates that the synthesized ZnO nanostructure is hexagonal. A sharp Zn-O vibration peak at 400~500 cm^{-1} confirms the presence of ZnO. The photoluminescence spectrum of ZnO nanostructure consists of a band-edge emission at 366 nm and visible light emission peaks due to defects. Based on the morphological information provided by scanning electron microscopy, transmission electron microscopy, and selected area electron diffraction, a growth mechanism for the formation of flower-like ZnO nanostructures is suggested. It only takes a few minutes to obtain ZnO nanostructures by the present approach.

Key words: ZnO; microwave combustion; nanostructure; photoluminescence

Zinc oxide (ZnO) is an important direct semiconductor with wide bandgap of 3.37 eV and large exciton bind energy of 60 meV at room temperature. Its unique optical, electronic, chemical, and thermal properties

收稿日期:2012-05-02。收修改稿日期:2012-08-17。
中央高校基础研究基金(No.CDJXS10221136)、科技部国际技术计划合作项目(1010104520100174)资助项目。
*通讯联系人。E-mail:caoyuan@cqu.edu.cn

have made ZnO a promising material in various fields, such as room-temperature ultraviolet lasers [1], field-effect transistors [2], photodetectors [3], gas sensors [4], photocatalysts [5], and solar cells [6]. To meet increasing demand for ZnO in these applications, efforts have been devoted to obtaining ZnO nanocrystals with controlled sizes and architectures because the optical, physicochemical, and electric properties of ZnO crystals are intimately dependent on their size and shape. Over the past decade, many interesting nanostructures of ZnO, such as nanorods[6], nanowires[7], nanorings [8], nanobelts [8], whisker [9], tetrapods [10], flowers[11], and nanospheres[12] have been fabricated. The latest investigations also indicate that a series of specific morphologies and structures of ZnO could possess even more novel properties. Huang et al. [1] observed room-temperature UV lasing in ZnO nanowire arrays and discovered that the nanostructure had a lower lasing threshold compared with disordered particles or films. Cao et al. [13] found that the energy conversion efficiency of dye-sensitized solar cells could be significantly enhanced using hierarchically structured nanosphere ZnO photoanodes. Through vertically aligned zinc oxide nanowire arrays, Wang et al. fabricated an ultrasonic wave-driven nanogenerator that produces continuous direct-current output[14].

To date, various synthetic methods, including hydrothermal synthesis [15], pyrolysis [16], the sol-gel technique [17], and chemical vapor deposition [18], have been developed to fabricate ZnO nanocrystals with controlled morphologies. However, most of the synthetic procedures available require expensive equipment and need to be operated under very strict conditions. Moreover, the synthesis of inorganic materials is time-consuming.

Compared with various techniques, the combustion synthesis method has many potential advantages, such as low-processing cost, energy efficiency, and time-saving features [19]. The microwave-induced combustion technique (MICT) is an economical method for preparing metal oxide materials. Metal nitrates and an organic compound, usually glycine (NH_2CH_2COOH) or urea [$CO(NH_2)_2$], are used as reactants. When igniting the aqueous solution of the reactants using microwave radiation, a combustion reaction takes place and transforms the reactants into a loose product composed of nanocrystalline particles. Y_2O_3[20], CeO_2[21], and TiO_2[22] have been successfully synthesized through MICT.

MICT induces the reactants to reach the reaction temperature fast through heating, and then the reaction takes place. During the process, including the dissolution of nitrate and fuel in a trace of water, the heated solution in the microwave oven decomposes a great deal of flammable gas, plenty of heat as well, reactants burn after reaching the self-ignition temperature. The whole reaction lasts for a few minutes, during which the nitrate plays the role of oxidant, urea and its cleavage product act as the reducing agents, and microwave induces the redox reaction. Nowadays there are relevant reports on Synthesizing inorganic materials based on MICT method. Nanocomposite NiO/YSZ powders for high performance anodes of SOFCs have been synthesized via a microwave-assisted complex-gel auto-combustion approach by Cai et al. [23] Sertkol et al. [24] also synthesized $Zn_{0.7}Ni_{0.3}Fe_2O_4$ nanoparticles via microwave assisted combustion route, and the product shows superparamagnetic behavior at around the room temperature and ferromagnetic behavior below the blocking temperature of 284 K.

Microwaves can be used to heat materials. As with all electromagnetic radiation, microwave radiation can be divided into an electric field component and a magnetic field component. The former is responsible for dielectric heating, which is effected via two major mechanisms [25]. One of the interactions of the electric field component with the matrix is called the dipolar polarization mechanism. And the other is the conduction mechanism. Microwave processing of materials is fundamentally different from conventional processing, such as the use of heating fluid, gas, steam, or electrical heating, due to its heating mechanism[26]. In a microwave oven, heat is generated within the sample by the interaction of microwaves with the material. In conventional heating, the heat is generated by heating elements. The heat is then transferred to the samples surfaces. Based on these details, we speculate that the

nanostructures or properties of as-synthesized ZnO would change after microwave radiation.

In this study, the MICT method is developed for the flash synthesis of ZnO crystals. The development of the MICT method is described and the effects of several experimental parameters on product quality are discussed. The morphologies necessary to form flower-like ZnO with different lengths of time are observed. We also suggest a mechanism of formation of flower-like ZnO, and evaluate the photoluminescence properties of the ZnO nanostructures.

1 Experimental

1.1 Materials and methods

All chemicals (analytical grade reagents) were commercially available and used without further purification. The MICT method involved the dissolution of zinc nitrate [$Zn(NO_3)_2 \cdot 6H_2O$] as an oxidizer, and fuel (urea [$CO(NH_2)_2$]) as a reducer in water. The resulting solution was heated in a microwave oven. Experimental details are as follows. Approximately 6 g of $Zn(NO_3)_2 \cdot 6H_2O$ was dissolved in 2 mL distilled water in a porcelain crucible. Urea was assembled in an appropriate proportion to form into fuel compounds. The fuel compounds were mixed well with the stock zinc nitrate solution until a ropy paste (hereafter termed as the precursor) was obtained. The precursor was introduced into a microwave oven (Galanz D8023CSL-K4), and a microwave field of 2.45 GHz was applied to it for decomposition to take place. After boiling, evaporating, and concentrating, the precursor foamed up, deflagrated, and released a certain amount of heat and gases. Microwave radiation was not stopped until the flame was extinguished. Combustion was completed within only a few minutes, and ZnO nanoparticles remained as residues.

The relative chemical reaction equation can be written as:

$$Zn(NO_3)_2 \cdot 6H_2O(c)+\Phi CO(NH_2)_2(c)+(1.5\Phi-2.5)O_2(g)\rightarrow ZnO(c)+(1+\Phi)N_2(g)+\Phi CO_2(g)+(6+2\Phi)H_2O(g) \quad (1)$$

Where c=crystal, g=gas

According to the concepts of propellant chemistry, in Eq. (**1**), $1.5\Phi-2.5=0$ corresponds to the situation where "the reactant composition was set at the condition equivalent to the stoichiometric ratio", which implies that the oxygen content of zinc nitrate could be completely reacted to oxidize fuels equivalently without demanding oxygen from any external source. Both the rates of reaction and the heat liberated per unit of time are at a maximum under this condition. Referring to Eq. (**1**), three representative reactant compositions were selected to synthesize ZnO products: (1) $\Phi=1$ is defined as deficient fuel; (2) $\Phi=1.667$ is defined as suitable fuel; and (3) $\Phi=3$ is defined as excess fuel. These also represented the relations between Zn^{2+} concentration and amount of fuel.

1.2 Characterization

The precursor powders were investigated using thermogravimetric analysis (TGA) and differential thermal analysis (DTA) between room temperature and 800 ℃ using a Shimadzu DTG-60H instrument. Analyses were performed under a nitrogen atmosphere at a temperature ramp of 10 ℃·min^{-1}. The obtained samples were characterized by infrared spectroscopy (FTIR) (Shimadzu Affinity-1 FTIR spectrophotometer in the range of 2 000~400 cm^{-1} using KBr pellets) and X-ray diffraction (XRD) (Shimadzu XRD-6000 with Cu $K\alpha$ radiation, $\lambda=0.154\ 18$ nm; diffractograms were obtained under the following conditions: $2\theta=20°\sim80°$, voltage of 40 kV, current of 40 mA, and scanning speed of 2°·min^{-1}). The morphologies and size of the products were investigated by scanning electron microscopy (SEM) (JEOL JSM-6490LV), field emission scanning electron microscopy (FESEM) (FEI Nova-400), and transmission electron microcopy (TEM) (JEOL JEM-2000EX) combined with selected area electron diffraction (SAED). The room-temperature PL was measured with a fluorescence spectrophotometer (Shimadzu RF-5301PC using a Xe laser with a wavelength of 325 nm as the excitation light source).

2 Results and discussion

2.1 Phenomena analysis

Fuels have an important effect on combustion reactions and the properties of the as-synthesized products because of the main energy released from the

exothermic reaction between fuels and zinc nitrate, which could rapidly heat the system to high temperatures and ensure that synthesis occurs. Therefore, depending on the amount of urea contained in the reactant compartment, three different kinds of reaction phenomena are observed. At low $CO(NH_2)_2$ contents (Φ=1), heat release is relatively low because of fuel scarcity. Thus, the precursor cannot deflagrate and the product color is not uniform. In the middle of the porcelain crucible, some pink powders containing harder agglomerates are obtained, whereas the white unreacted precursor is left near the vessel wall. The low temperature of the vessel wall is not enough to trigger significant changes. In the case of $CO(CH_2)_2$ (Φ=1.667 and Φ =3), liberation of the energy during the combustion reaction is enough to ignite the precursor. A stable flame is observed after smoke evolution. Pink powder agglomerates are obtained at Φ=1.667, whereas light yellow color powders in loose shapes are obtained at Φ=3.

The response characteristic for the shortage of fuel is a slower reaction rate and lack of substantial flame. By contrast, the great response rate exists in the reaction of fuel abundance and the reaction is almost completed at the same time. Under this condition, all the oxygen comes from the precursor. Once NO_3^- creates oxygen, it immediately reacts with urea. With increasing fuel content, the key reason for obtaining loose-shaped products is the liberation of a large amount of gases during combustion. The gases hamper the subsequent condensation of particles. When the fuel is in excess, the combustion reaction must be taken outside to increase oxygen. Therefore, the critical factor that limits reaction rates is the amount of oxygen in the system, which enters the reaction zone by diffusion.

TGA and DTA curves of the ZnO precursor are shown in Fig.1. The major weight loss occurs at about 310 ℃, and the minor ones at temperatures between 420 and 500 ℃. The mass remains constant at higher temperatures, indicating oxide formation. A weight loss of about 70% is observed, corresponding to the evolution of absorbed moisture (water and other low molecular weight compounds), the burning out of

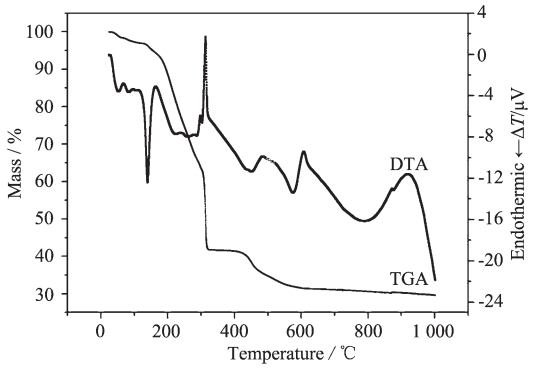

Fig.1　TGA-DTA curves of the precursor

carbon dioxide, and the presence of excess nitrate gases in the as-prepared precursor ZnO powder. The DTA curve shows the three steps in the decomposition behavior of exothermic peaks between room temperature and 1 000 ℃. First, a broad peak below 200 ℃ corresponds to the desertion of moisture from the precursor powder and removal of water molecules from the hydroxyl group. The exothermic peaks in the 300~700 ℃ range correspond to the volatile product (CO_x, N_2, NO_x, etc.) formation and organic material combustion. The broad peak at about 900 ℃ could be attributed to the crystal phase transition of ZnO. TGA and DTA data display the transformation of precursors in the microwave oven.

2.2　Crystal structure and functional group analysis

The XRD patterns of zinc oxide nanopowders prepared by the MICT are shown in Fig.2. The sharp diffraction peaks match the pattern of the standard

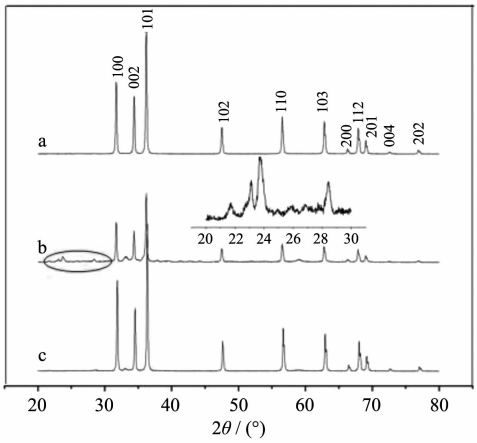

(a) 1:1; (b) 5:3; (c) 3:1

Fig.2　XRD patterns of ZnO samples with the following molar ratios of urea/Zn^{2+}

hexagonal structure of ZnO (PDF No. 36-1451), with lattice constants a=0.324 9 nm and c=0.520 6 nm. The strongest peaks located at 31.72°, 34.40°, and 36.18° can be clearly seen and correspond to the (100), (002), and (101) directions of ZnO, respectively. Besides the three most obvious peaks, other peaks representing (102), (110), (103), (200), (112), (201), (004), and (202) directions of ZnO can also be indexed from the ZnO (PDF No. 36-1451). No secondary peaks are detected in Figs.2a and 2c, indicating the complete crystallization of single phase hexagonal ZnO. However, comparison of the curve of Fig.2b with those of Figs.2a and 2c show some weak peaks located at 21°~29° (inset, Fig.2b). These peaks indicate that a rapid reaction is not conducive to the formation of the single phase ZnO.

The formation of ZnO nanostructures is further characterized by FTIR spectroscopy, as shown in Fig.3. The absorption at ~1 383 cm^{-1} for the synthesized samples corresponds to the bending vibration of C-N. This indicates the presence of nitrate ions, which are probably absorbed on the surface of ZnO particles. The intense band that rises at 400~500 cm^{-1} in all the spectra is assigned to the stretching vibrations of Zn-O. A sharp Zn-O vibration peak at 449 cm^{-1} appears with a urea/Zn^{2+} molar ratio of 3∶1, and the single peak is attributed to a comparatively large amount of heat energy and the higher temperature. The peaks observed in the FTIR spectra of the powders are found to match well with those previously reported[27].

2.3 ZnO nanostructures

Fig.4 shows the SEM and FE-SEM images of the ZnO nanostructures prepared by the MICT at different molar ratios of urea/Zn^{2+}. When the molar ratio of urea/Zn^{2+} is equal to 1, nanostructure flowers can be obtained at all three microwave powers (170, 340, and 680 W), as shown in Fig.4. However, the flowers are not fully formed when the microwave power is too low (Fig.4a), and the size of the flower clusters is inhomogeneous (Fig.4c). Moreover, the higher the microwave power, the shorter the time for the occurrence of deflagration. Since a short reaction time is not beneficial to crystal nucleation and growth, moderate microwave radiation power (340 W) is selected to investigate the effect of organic fuels on the nanostructures. Results show that uniform flower-like products are obtained with a 1∶1 molar ratio of urea/Zn^{2+}, as shown in Fig.4b and 5a. The product consists of a large quantity of flower-like microstructures that are approximately 2~5 μm in size. The floral structures result from the accumulation of several hundreds of sharp-tipped ZnO nanorods, which originate from a single center. A urea/Zn^{2+} molar ratio of

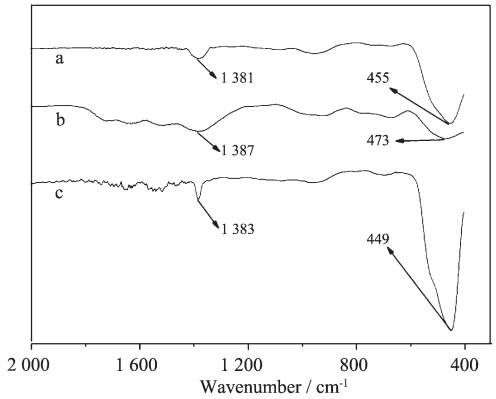

(a) 1∶1; (b) 5∶3; (c) 3∶1

Fig.3 FTIR spectra of ZnO samples with the following molar ratios of urea/Zn^{2+}

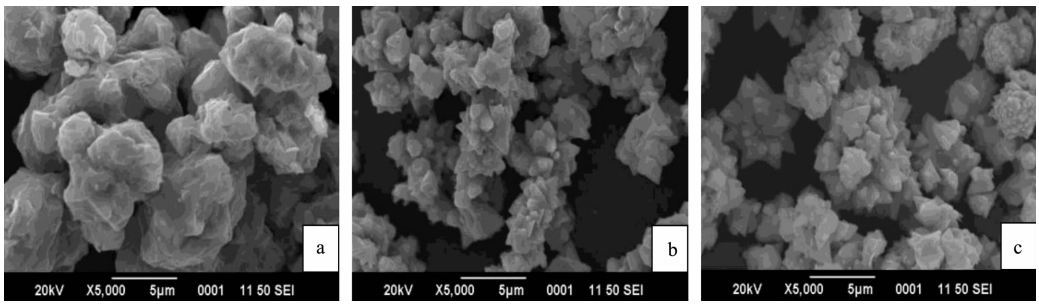

(a) 170 W; (b) 340 W; (c) 680 W

Fig.4 SEM images of ZnO samples with a 1∶1 molar ratio of urea/Zn^{2+} and at different microwave powers

5:3 results in incomplete flower-shaped nanostructures. As well, flakes agglomerate around the flowers (Fig.5b). The overall floral morphology fully changes into a blocky structure with a urea/Zn^{2+} molar ratio of 3:1, as shown in Fig.5c. The lengths of these irregular block-shaped particles range from 100~300 nm. The results illustrate that urea, rather than microwave power, acts as a structure-directing agent, significantly affecting the anisotropic growth of ZnO from flowers to block-like structures. Different single-crystal ZnO nanostructures are obtained after only a few minutes of microwave radiation.

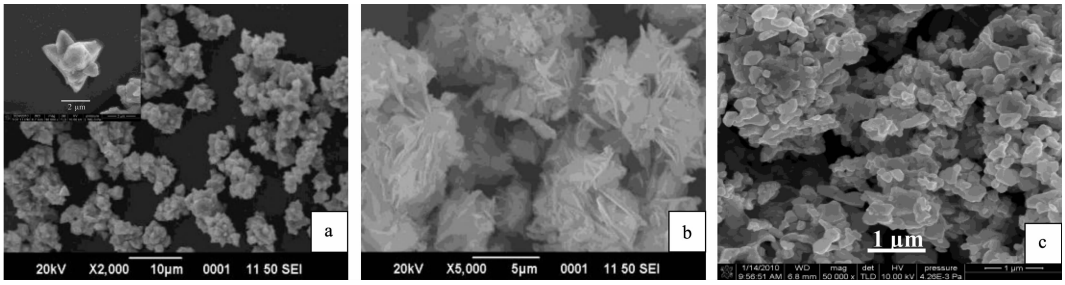

(a) 1:1; (b) 5:3; (c) 3:1

Fig.5　SEM images of ZnO samples at a microwave power of 340 W and with the following molar ratios of urea/Zn^{2+}

Fig.6a shows a low-magnification TEM image of flower-shaped ZnO, which is consistent with SEM observations (Fig.5a). The corresponding SAED pattern (Fig.6b) indicates that the structure evolves from poly-crystalline phases into single crystals. Characteristics of single-crystal diffraction spots and poly-crystalline diffusion rings can be seen from the SAED pattern. A high resolution TEM (HRTEM) image (Fig.6c) of the corresponding flowers clearly reveals that the lattice fringes between two adjacent planes are about 0.52 nm apart, which is equal to the lattice constant of ZnO, indicating that the obtained structures have wurtzite hexagonal phases and are preferentially grown along the (0001) direction. These findings are in accordance with the SAED pattern obtained.

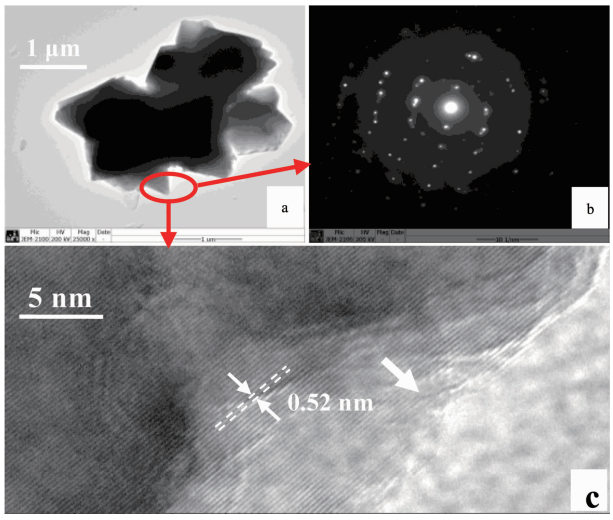

Fig.6　(a) TEM images of ZnO samples with a 1:1 molar ratio of urea/Zn^{2+}; (b) the corresponding SAED pattern; and (c) HRTEM image of individual ZnO nanorods in Fig.6(a)

2.4　Morphology evolution

In principle, the formation of 3D structures may be divided into two processes, i.e., nucleation and growth. In the experiments, urea mediates the nucleation and growth of ZnO crystals by modifying the basicity of the precursor solutions. The following chemical reactions take place in the precursor solutions:

$$H_2N\text{-}CO\text{-}NH_2+2H_2O \rightleftharpoons H^+\text{-}H_2N\text{-}CO\text{-}NH_2\text{-}H^++2OH^- \quad (2)$$

$$Zn^{2+}+2OH^- \rightleftharpoons Zn(OH)_2\downarrow \quad (3)$$

$$Zn(OH)_2+2OH^- \rightleftharpoons Zn(OH)_4^{2-} \quad (4)$$

$$Zn(OH)_4^{2-} \rightleftharpoons ZnO\downarrow+2OH^-+H_2O \quad (5)$$

Due to the hydrolysis of urea, the hydroxyl ion plays a crucial role in the nucleation process. At early stages of the reaction, ZnO nucleates from the $Zn(OH)_4^{2-}$ solution to form multi-nuclei aggregates. With constant stirring, the multi-nuclei aggregates serve as sites for ZnO nanostructure growth along the (001)direction. This direction has a high capability for inducing the nucleation of ZnO [28], according to the mechanism of polar crystal growth. In Fig.7a, the precursor solutions form the ZnO nanorods prior to microwave radiation. The similar phenomenon of ZnO crystal nucleus growth

in solution has been reported in several studies[29]. Due to molecular polarization in the reaction solution and the dipole moment formed in the dielectric, the level of excitation of Zn-O bonds is higher than normal under microwave radiation [30]. Thus, the material coupled in the microwave field heats up more rapidly than in a convectional heating system. After microwave radiation for 5 min, the reaction solution boils and becomes concentrated before burning. ZnO columns/rods are formed, as illustrated in Fig.7b. When the solution burns with a stable flame, flower-like single-crystal ZnO nanostructures are formed with rapid growth rate in the combustion process after the combustion reaction (Figs. 7c and 7d). The formation of flake-like ZnO and nanoparticles can be attributed to the liberation of large amounts of gases during combustion. A full description of these mechanisms would require more evidence from future work.

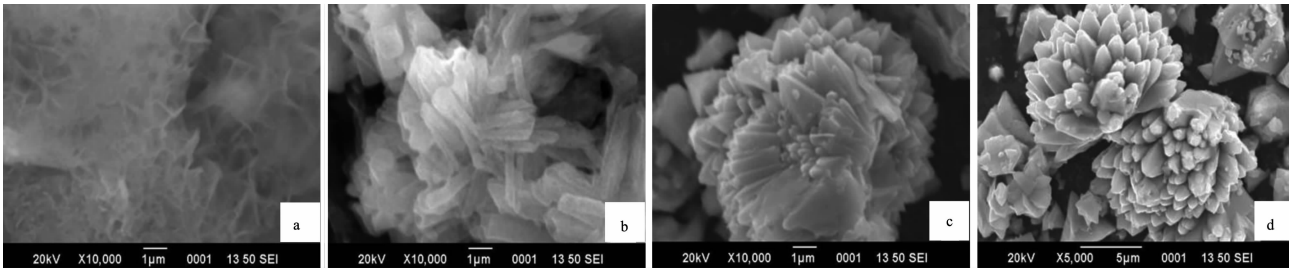

(a) precursor solutions before microwave radiation; (b) sticky reactants after microwave radiation, before burning; (c) powder just after the combustion reaction; and (d) powder under microwave radiation after burning

Fig.7 SEM images of flower-like ZnO structures in different phases

2.5 Photoluminescence studies

To investigate the effect of morphology on photoluminescence characteristics, the room temperature photoluminescence (PL) spectra of (a) flower-like, (b) flake-like, and (c) block-like ZnO are shown in Fig.8. The resulting ZnO nanopowders display an ultraviolet emission at 366 nm and a relatively broad blue light emission in the range of 380~500 nm.

The ultraviolet emission is attributed to the near band-edge emission of the wide band-gap ZnO, specifically, the recombination of free excitons through an exciton-exciton collision process[31]. The emission at 366 nm is frequently observed in ZnO thin films deposited on gold substrates[32]. Lin et al. found violet emissions at 390 nm (3.18 eV) during the DC reactive sputtering of ZnO films onto Si substrates [33]. They believe that the violet emission originates from the electron transition from the conduction band to the valence band. We believe that the emission at 394 nm is due to the electron transition from the conduction band tail states to the valence band tail states. The 410 nm violet luminescence is thought to relate to interface traps at the grain boundaries and emissions from the radiative transition between this level and the valence

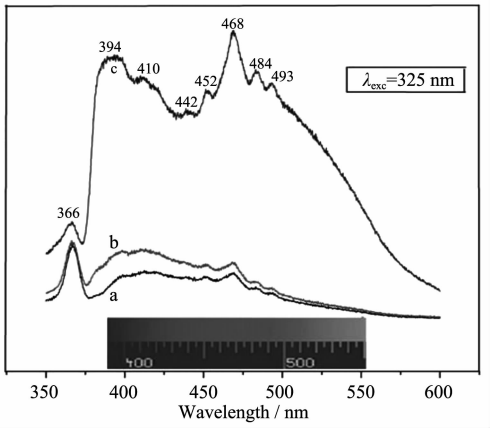

(a) 1:1; (b) 5:3; (c) 3:1

Fig.8 PL spectra of ZnO samples at a microwave power of 340 W and with the following molar ratios of urea/Zn^{2+}

band[34]. Teng et al.[35]believe that this emission could be due to the transition from the top of the valence band to the Zn_i level (interstitial zinc, 2.9 eV). A weak blue emission at 442 nm (2.81 eV) was observed in the ZnO nanoflowers; this emission has also been found in ZnO films and whiskers[36]. Previous studies on ZnO films prove that the blue emission is related to oxygen vacancies in the ZnO film[37]. The 452 nm (2.74 eV) emission is assigned to rather shallow donor level of Zni

recombined with V_{Zn} (vacancies zinc) by recent study[38-39].The 468 nm (2.64 eV) emission is not widely observed, although it is usually considered to be related to intrinsic defects generated during the preparation and post-treatment of nanostructures, such as single negatively charged zinc vacancies, the origins of which remain unclear. The hump at 485 nm in the PL spectra of ZnO can be attributed to the transition between the vacancies of oxygen and interstitial oxygen[40]. Such an emission can also result from surface-deep traps, which are typical of porous ZnO nanostructures [41]. The shoulder peak at 493 nm is related to singly ionized oxygen vacancies. This emission results from the recombination of a photogenerated hole with a singly ionized charge state of the specific defect[42]. The green luminescence (500~550 nm) of ZnO nanostructures is not obvious. The peak intensity of the sample obtained at the urea/Zn^{2+} molar ratio of 3:1 is stronger than that at 1:1. It is possible that the surface defects contribute to the emission because the block-like nanoparticles have smaller size and larger surface area. Zhang et al. [43] reported that surface states may play a more important role in visible emissions than previously thought. Hence, in our case, it may be reasonably inferred that both oxygen vacancies and surface states may respond to the yellow-green emission of the flower-like ZnO nanorods.

The origins of different defect emissions are not completely understood, but we can speculate that differences in the optical properties of the present ZnO nanostructures originate from lattice defects related to either the oxygen interstitial spaces or Zn vacancies.

3 Conclusions

A rapid and simple method was developed for preparing flower-like ZnO nanocrystals through the MICT. Results reveal that the molar ratio of urea/Zn^{2+} significantly influences the morphology of ZnO. The effect of ZnO morphologies is attributed to the induction of hydroxyl ions, which orients nucleation and promotes rapid growth under microwave radiation. Our results reveal that ZnO nanorods are created from ZnO nuclei, resulting in the formation of flower-like ZnO nanostructures. Photoluminescence spectra of ZnO flowers, flakes, and block-like nanostructures reveal several emission bands. The distinctive advantage of the proposed method is that the process requires no heat treatment or calcination at high temperature.

References:

[1] Huang M H, Mao S, Feick H, et al. *Science*, **2001**,**292**: 1897-1899

[2] Yuan H, Shimotani H, Tsukazaki A, et al. *Adv. Func. Mater.*, **2009**,**19**:1046-1053

[3] Al-Hardan N H, Abdullah M J, Ahmad H, et al. *Sol. St. Electr.*, **2011**,**55**:59-63

[4] Anderson T, Ren F, Pearton S, et al. *Sensors*, **2009**,**9**:4669-4694

[5] Yang J L, An S J, Park W I, et al. *Adv. Mater.*, **2004**,**16**: 1661-1664

[6] Zhang R, Kumar S, Zou S, et al. *Cryst. Growth Des.*, **2008**,**8**: 381-383

[7] Pung S Y, Choy K L, Hou X, et al. *Nanotechnol.*, **2010**,**21**: 345-602

[8] Pan Z W, Dai Z R, Wang Z L. *Science*, **2001**,**291**:1947-1949

[9] Qiu Z, Wong K S, Wu M, et al. *Appl. Phys. Lett.*, **2004**,**84**: 2739-2741

[10]Wang Q, Yu K, Wang T H, et al. *Appl. Phys. Lett.*, **200**3, **83**:2253-2255

[11]Cao Y, Liu B L, Huang R, et al. *Mater. Lett.*, **2011**,**65**:160-163

[12]Zhang Y, Liu Y, Wu L, et al. *Appl. Surf. Sci.*, **2009**,**255**: 4801-4805

[13]Chou T P, Zhang Q, Fryxell G E, et al. *Adv. Mater.*, **2007**, **19**:2588-2592

[14]Wang X, Song J, Liu J, et al. *Science*, **2007**,**316**:102-105

[15]Zhang H, Yang D, Ji Y, et al. *J. Phys. Chem. B.*, **2004**,**108**: 3955-3958

[16]Puspharajah P, Radhakrishna S. *J. Mater. Sci.*, **1997**,**32**: 3001-3006

[17]Shan G, Xiao X, Wang X, et al. *J. Colloid Interface Sci.*, **2006**,**298**:172-176

[18]Wu J J, Liu S C. *Adv. Mater.*, **2002**,**14**:215-218

[19]Mangalaraja R V, Mouzon J, Hedstrm P, et al. *J. Mater. Process. Tech.*, **2008**,**208**:415-422

[20]Mangalaraja R V, Mouzon J, Hedstrm P, et al. *Powder Technol.*, **2009**,**191**:309-314

[21]Fu Y P, Lin C H, Hsu C S. *J. Alloys Compd.*, **2005**,**391**: 110-114

[22]Gressel-Michel E, Chaumont D, Stuerga D. *J Colloid Interface Sci.*, **2005**,**285**:674-679

[23]Sertkol M, Köseolu Y, Baykal A, et al. *J. Magn. Magn. Mater.*, **2010**,**322**:866-871

[24]Cai T X, Zeng Y W, Zhang W, et al. *J. Power Sources*, **2010**,**195**:1308-1315

[25]Lidström P, Tierney J, Wathey B, et al. *Tetrahedron*, **2001**, **579**:225-283

[26]Fu Y P, Su Y H, Lin C H. *Solid State Ionics*, **2004**,**166**:137-146

[27]Fernandes D M, Silva R, Winkler Hechenleitner A A, et al. *Mater. Chem. Phys.*, **2009**,**115**:110-115

[28]Sun Y, Riley D J, Ashfold M N R. *J. Phys. Chem. B*, **2006**, **110**:15186-15192

[29]Feng L, Liu J, She J J. et al. *Cryst. Growth*, **2009**,**311**:1435-1440

[30]Tompsett G A, Conner W C, Yngvesson K S. *Chem. Phys. Chem.*, **2006**,**7**:296-319

[31]Kong Y C, Yu D P, Zhang B, et al. *Appl. Phys. Lett.*, **2001**,**78**:407-409

[32]Laurent K, Wang B Q, Yu D P, et al. *Thin Sol. Films*, **2008**,**517**:617-621

[33]Lin B, Fu Z, Jia Y. *Appl. Phys. Lett.*, **2001**,**79**:943-945

[34]Wang Y, Chu B. *Superlattice Microst.*, **2008**,**44**:54-61

[35]Teng X M, Fan H T, Pan S S, et al. *J. Phys. D*: *Appl. Phys.*, **2006**,**39**:471-476

[36]Dai L, Chen X L, Wang W J, et al. *J. Phys.*: *Condens. Mat.*, **2003**,**15**:2221-2226

[37]Bachari E M, Baud G, Amor S B, et al. *Thin Sol. Films*, **1999**,**348**:165-172

[38]Patra M K, Manzoor K, Manoth M, et al. *J. Lumin.*, **2008**, **128**:267-272

[39]Chawla S, Karar N, Chander H. *Phys. B* (*Amsterdam, Neth.*), **2010**,**405**:198-203

[40]Mahamuni S, Borgohain K, Bendre B S, et al. *J. Appl. Phys.*, **1999**,**85**:2861- 2865

[41]Song R Q, Xu A W, Deng B, et al. *Adv. Funct. Mater.*, **2007**,**17**:296-306

[42]Tian Y, Lu H B, Wu Y, et al. *Mater. Sci. Tech-Lond.*, **2010**, **26**:1248-1252

[43]Zhang H, Shen L, Guo S W. *J. Phys. Chem. C*, **2007**,**111**: 12939-12943